Wave-equation tomography - II

F. Rocca and Marta J. Woodward

ABSTRACT

Using simple geometrical techniques, we analyze the Fourier spectrum of the backprojection of an acoustical wavefield gnerated by a point source and recorded by a point geophone. We show that the spatial width of the backprojection, in the seismic range of frequencies (the width of the seismic ray), is not negligible so that it is useful to consider the effects of dispersion due to lateral inhomogeneities of the medium. We then show the correspondence between bandpassed traveltimes analysis and the Rytov approximation; finally, we analyze the null space of the extended traveltimes inversion and find that it is dependent on the time windowing of the reflected arrivals.

INTRODUCTION

Wave-equation migration techniques have recently been re-analyzed in terms of inversion theory (Cheng and Cohen, 1984). A satisfying situation appears to have been reached. Actual industrial practice can be seen as the first of a series of steps that can lead to full inversion of the data set: i.e., determination of the petrophysical properties of rocks, consistent with recorded data and with a priori hypotheses based on geological judgment. Seismic velocity analysis is still far from this optimum frame; it has been extended to two-dimensional media by means of the technique known as seismic tomography. Traveltimes of reflections are used as constraints to determine the interval velocities of the inhomogeneous medium. It is not yet clear what can be obtained from inversion, in that eigenvectors and eigenvalues of the matrix relating interval velocities to measured traveltimes depend on the position of the reflectors. This leads to unavoidable ambiguities. Moreover, the use of geometric acoustics does not clearly identify the null space of the transformation, and causes problems in the inversion as a result. From one side, wavenumbers of the object spectrum are, in fact, inverted where no information is really available, generating artifacts and instabilities that must be removed via ad hoc smoothing techniques. On the other side, the data are not used optimally. Traveltimes are only a crude approximation of the action of the scatterers on the waveshape of the first arrivals; lumping all available information into a single number, i.e. the differential traveltime with respect to the unperturbed ray, entails losing data that could be very useful for the successive inversion.

The aim of this paper is to use diffraction tomography, as introduced by Devaney in the early 80's (Devaney, 1982, 1983), to establish a bridge between ray tracing and first arrival inversion techniques based on the wave-equation. Up to now, diffraction tomography has been mostly analyzed in the wavenumber domain. As the ultimate goal of our work is an inversion of the bandpassed traveltimes of the seismic reflections, we transferred the analysis of diffraction tomography to the space domain, in order to be able to select couples of sources and geophones and to window events in time. As in seismic tomography, our data will be mostly nonlinearly related to the recorded wavefield, even if the nonlinearity will not be as crude as the traveltime picking process. Moreover, we shall make use of the wave-equation. Hence, the name wave-equation tomography is given to the process.

Using only very elementary techniques, so that we will be able to be completely supported along the way by physical intuition, we shall analyze the effects of Born and Rytov approximations techniques (Born, 1959; Rytov, 1937). These techniques approximate how the scatterer's distribution affects the phases, amplitudes, and then traveltimes of the wavefield. The results of the analysis will indeed be that ray tracing and traveltime inversion on one side neglects the existence of a quite noticeable null space induced by the limited cable and survey length. All available data are not used, on the other side.

This paper is organized as follows: we first derive the Fourier transform of the monochromatic backprojection using elementary geometry. We do so to avoid obscurities deriving from complex mathematics. Monochromatic backprojection is defined as the most probable distribution of scatterers consistent with a single frequency measurement for a single couple of source and geophones. We then extend this analysis to multiple frequencies and to multiple locations of sources and geophones. From the multifrequency analysis we are able to derive the width of the ray, i.e., the lateral extension of the area where we can impose a constraint on the scatterer's distribution if the transfer function between source and geophone is a pure delay. We shall see that this width is independent of the central frequency of the radiation, and is inversely proportional to the bandwidth of the measurement, an intuitively satisfying fact. After a short summary of the Rytov approximation, and presentation of a simple example of its implications, we shall then see how seismic-traveltime tomography can be linked to the wave-equation via the diffraction tomography of the seismic sources reflected by plane layers and the Rytov approximation. We shall see how traveltime inversion is only a crude approximation. Moreover, we shall see that it is not possible to consider the reflected sources to be identical to real buried sources; we cannot apply diffraction tomography to them without some time window. The time windowing is aimed at selecting events consistent with the hypothesized travelpaths.

This paper is meant to complement another, in this volume (Woodward, 1988), which presents many of the same ideas from a different viewpoint along with numerical

numerical examples.

SCATTER IN THE WAVENUMBER DOMAIN

Let us consider a monochromatic source radiating acoustic energy at frequency ω. In the (x,y) plane Source S is located in (-D/2,0); Geophone G is located in (D/2,0). The scatterer varies sinusoidally with the space coordinates; it is thus characterized by a single wavenumber in the Fourier domain of the object (Figure 1).

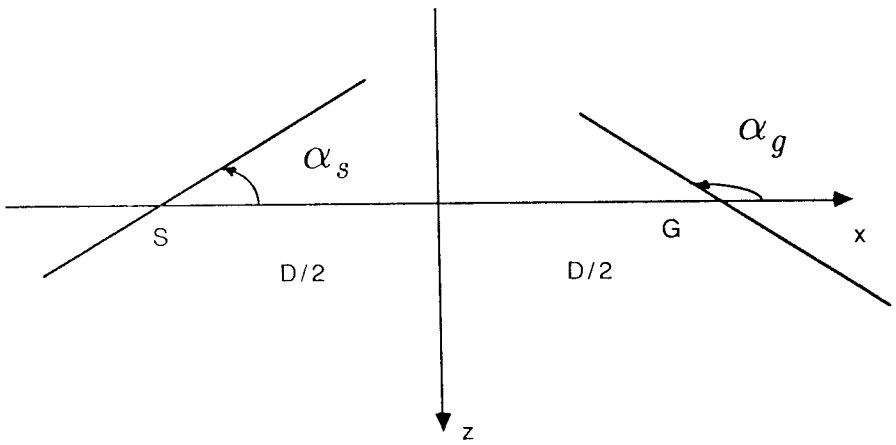

FIG. 1. Location of source and geophone in the uniform medium.

If we decompose (Devaney, 1982, 1983; Miller et al., 1987; Wu and Toksoz, 1987) the source signal into planar waves that make real angles with the coordinate axes we have:

$$\psi_s(t) = \exp j(-\omega t + u_s(x + D/2) + v_s y) \tag{1}$$

where u_s , v_s are the components of the wavevector of the signal generated at the source location. We postpone the mathematical analysis of the complex angles and evanescent waves to a later occasion. Let the scatterer be:

$$r(x,y) = Ae^{j\phi_0}\exp j(u_0 x + v_0 y). \tag{2}$$

We will suppose that the scatterer is very weak, so that we can superpose effects; thus, we can keep the reflectivity complex. A real reflectivity will be obtained by combining two conjugate functions. The scattered field measured at the geophone site is:

$$\psi_s(D/2) = Ae^{j\phi_0}\exp j[(u_0+u_s)D/2+u_s D/2-\omega t]. \tag{3}$$

The phase difference between the scattered field and the source is

$$\phi_s = D\,(u_s + u_0/2) + \phi_0. \tag{4}$$

Defining

$$u_g = u_s + u_0 \;\; ; \;\; v_g = v_s + v_0 \tag{5}$$

and using polar coordinates, we now have

$$u_s = -\frac{\omega}{c}\sin\alpha_s \quad u_g = -\frac{\omega}{c}\sin\alpha_g \quad v_s = \frac{\omega}{c}\cos\alpha_s \quad v_g = \frac{\omega}{c}\cos\alpha_g\,, \tag{6}$$

where α_s and α_g are the real angles that the incident and the scattered wave make with the x axis. Equation (5) becomes:

$$u_0 = 2\frac{\omega}{c}\sin\frac{|\alpha_s - \alpha_g|}{2}\cos\frac{(\alpha_s + \alpha_g)}{2} = \rho\cos\theta \tag{7}$$

$$v_0 = 2\frac{\omega}{c}\sin\frac{|\alpha_s - \alpha_g|}{2}\sin\frac{(\alpha_s + \alpha_g)}{2} = \rho\sin\theta,$$

where (Figure 2)

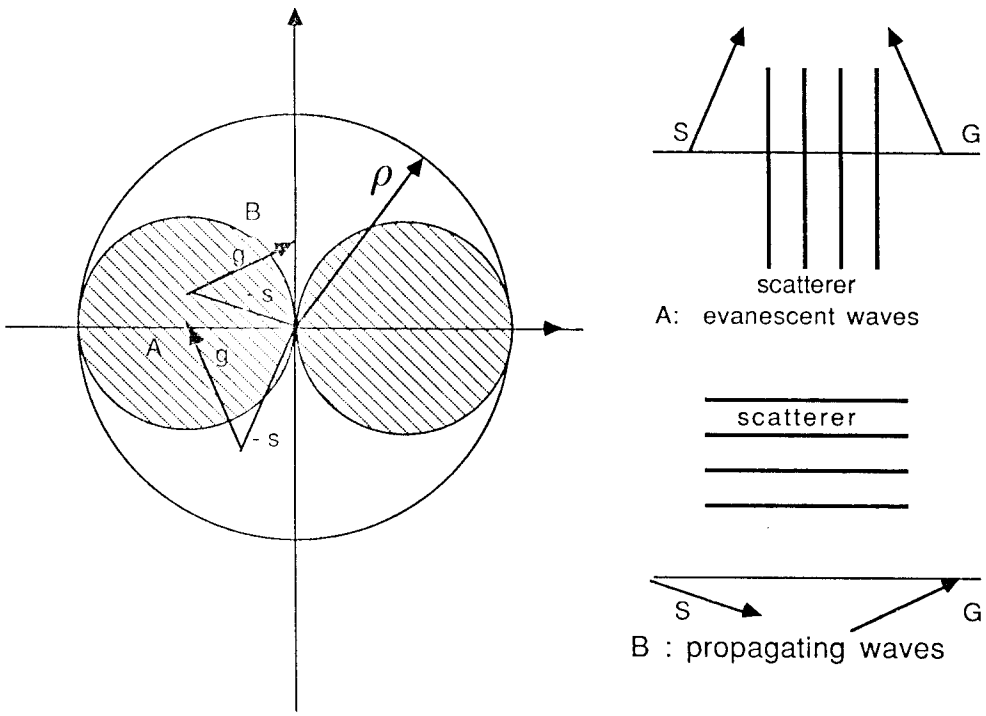

FIG. 2. Scatterers in the wavenumber domain.

$$\rho = 2\frac{\omega}{c}\sin\frac{|\alpha_s - \alpha_g|}{2} \tag{8}$$

$$\theta = \frac{\alpha_s + \alpha_g}{2}.$$

The Jacobian of the transformation from α_s , α_g to u_o , v_o is:

$$J = \frac{\omega^2}{c^2}\sin|\alpha_s - \alpha_g| = \frac{\omega}{c}\rho\sqrt{1-\frac{c^2\rho^2}{4\omega^2}}. \tag{9}$$

This implies that if we have an uniform distribution of the source angles (isotropic point source), and wish the radiation impinging on the geophone to have no preferential directions, then the distribution of the scatterers' wavenumbers should peak at ρ=0 and ρ=$2\omega/c$. In fact, the spectrum should be proportional to the inverse of J. If we measure a phase ϕ_s at the geophone, then the phase of a candidate scatterer at the spatial frequency that has polar coordinates ρ and θ is :

$$\phi_0 = \phi_s - \frac{D}{2}(u_s + u_g) = \phi_s + \frac{\omega}{c}D\sin\theta\sqrt{1-\frac{c^2\rho^2}{4\omega^2}}. \tag{10}$$

Equations (9) and (10) provide the basis for the determination of amplitude and phase respectively of the Fourier anti-transform of the monochromatic backprojection that we will discuss in the next section.

THE MONOCHROMATIC BACKPROJECTION

We have seen in the previous section that if there is a sinusoidally-varying scatterer like the one represented in equation (2), then we will measure a signal with the phase given by (10). On the other hand, if we measure a phase ϕ_s and let it be zero without loss of generality, equation (10) gives the phases of the candidate scatterers (in the spectral domain) congruent with that measurement. We will obviously be unable to determine the wavenumber of the scatterer if we hypothesize isotropic sources and geophones. Rather, we have to recur to the same sort of statistical argument that is used for tomography and for diffraction-scatter summation. If we have an impulsive source and receive a pulse at time T, then we can hypothesize a distribution of scatterers along the ellipse with foci in S and G and major axis length cT. We assume that the scatterers in all other locations have zero amplitude. Similarly, we could now suppose we have scatterers with wavenumbers in the circle with radius $2\omega/c$ with phases according to (10) and amplitudes according to 1/J. The scatterers will be reconstructed superposing the backprojections from measurements at different frequencies and locations of sources and geophones. Further criticism is necessary to determine the effects of windowing in the spatial as well as in the wavenumber domain. Moreover, the causality condition implied by the point sources has to be applied, and will have important consequences for the reconstruction.

Using elementary techniques, we analyze the spatial structure of the anti-transform of the function characterized by the phase function of (10). The discussion is implied by results that have recently been obtained in three dimensions by Tygel and Hubral (1985) and in two dimensions by Wengrovitz and Oppenheim (1987). This derivation offers the advantage of providing geometric insight; it establishes a bridge with diffraction tomography.

An easy way to estimate the anti-transform of (9) is to calculate, for each θ, ρ the gradient of the phase (the equivalent of the group delay) with respect to u_o , v_o , or in polar coordinates, with respect to ρ and θ. Rewriting (10), with ϕ_s =0, we have:

$$\phi_0(\rho,\theta) = + \frac{\omega}{c} D \sin\theta \sqrt{1-\frac{c^2\rho^2}{4\omega^2}}. \tag{11}$$

Normalizing the frequency scale with respect to $2\omega/c$, and the length scale to D/2, we have, in that scale and neglecting the subscript,

$$0 < p = \frac{\rho c}{2\omega} < 1 \tag{12}$$

$$\phi = \sin\theta\sqrt{1-p^2}.$$

The components of the gradient in polar coordinates are

$$\frac{\partial\phi}{\partial p} = - \frac{p}{\sqrt{1-p^2}}\sin\theta = - q \sin\theta \tag{13}$$

$$\frac{1}{\rho}\frac{\partial\phi}{\partial\theta} = \frac{\cos\theta}{q}$$

$$q = \tan\frac{|\alpha_s - \alpha_g|}{2} = \frac{p}{\sqrt{1-p^2}}.$$

If we call ξ , η the spatial cooordinates of the point of the plane identified by the gradient, in the wavenumber domain we have:

$$\xi = - q \sin\theta\cos\theta - \frac{1}{q}\sin\theta\cos\theta \tag{14}$$

$$\eta = - q \sin^2\theta + \frac{\cos^2\theta}{q}.$$

The anti-transform in ξ , η is directed along a line orthogonal to the direction θ locally. If we now pose

$$q = \sqrt{\frac{a^2}{\sin^2\theta}-1} \tag{15}$$

$$p = \sqrt{1-\frac{\sin^2\theta}{a^2}},$$

the family of curves described by equation (14) for different values of a will be a set of

confocal conics, with foci in +1 and - 1, (the location of source and geophone in the scaled coordinates), and equation:

$$\frac{\xi^2}{a^2} + \frac{\eta^2}{a^2-1} = 1. \tag{16}$$

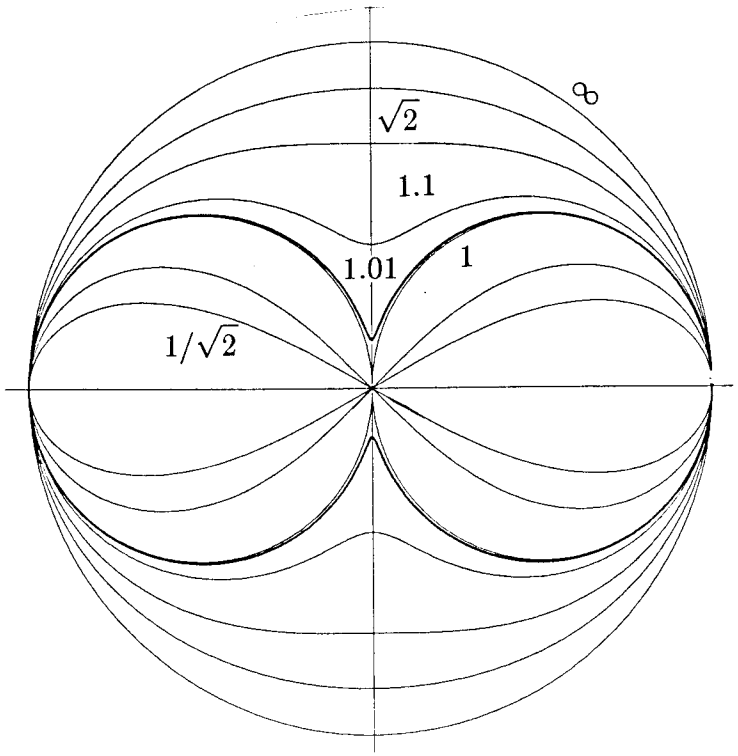

FIG. 3. Migration ellipses in the wavenumber domain ($a > 1$). Values of a smaller than 1 correspond to nonphysical hyperbolas. The outer circle corresponds to zero offset or to $a = \infty$.

These curves (Figures 3 and 4) are ellipses when the parameter a is greater then 1, and hyperbolae otherwise. The value $a = 1$ corresponds to the straight line linking S to G. The sine of the half offset angle β (Claerbout, 1985) can be seen to be equal to $\sin\theta/a$. Therefore, if we look at Figure 5 we see that the hatched region corresponds to the hyperbolae, i.e. loci of time subtraction rather than time addition. In other words, in this region the direction of the plane wave propagating from the source, impinging on the sinusoidal scatterer, and returning to the geophone implies a retrograde path, i.e. corresponding to evanescent waves (Figure 2). The other region corresponds to the physical backprojection, i.e. to a set of monochromatic ellipses.

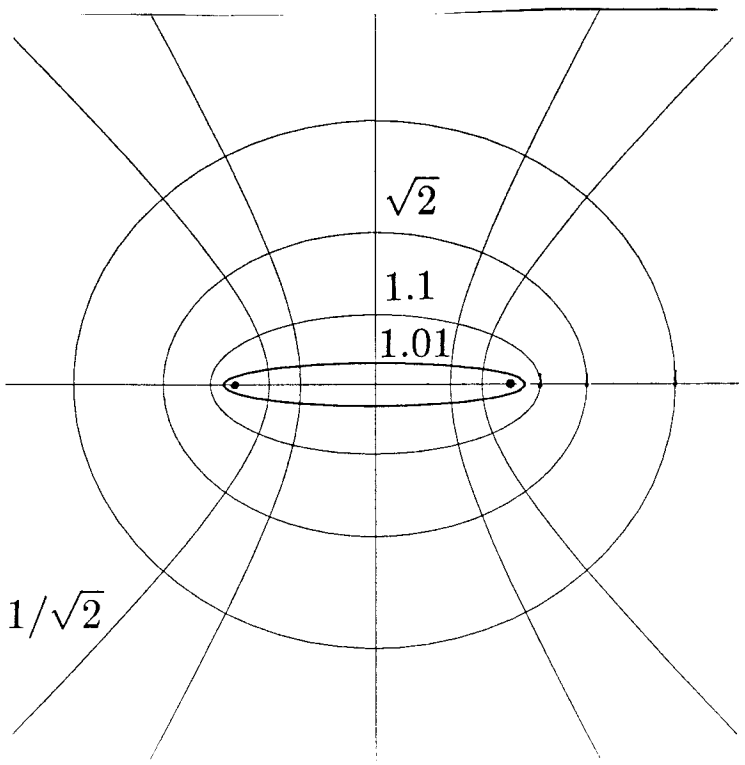

FIG. 4. Migration ellipses in the space domain. The hyperbolas ($a < 1$) correspond to non physical arrivals.

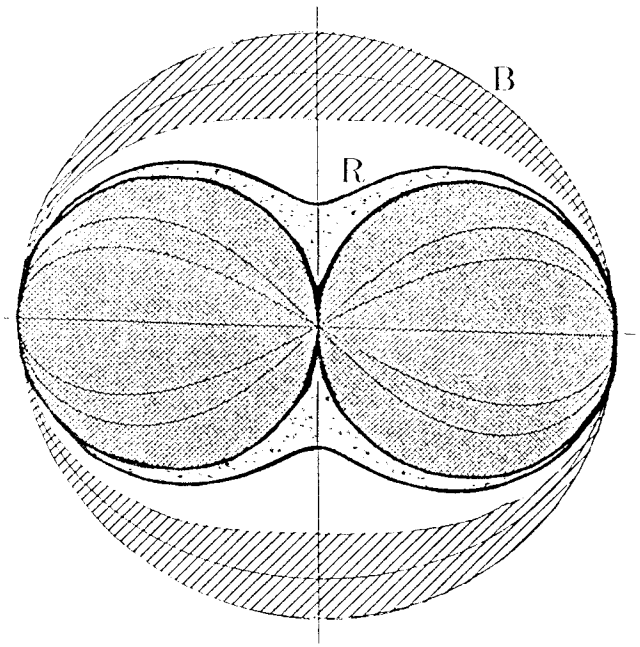

FIG. 5. Born and Rytov regions in the wavenumber domain. Region B (dashed) corresponds to values of a greater than $\sqrt{2}$; region R (dotted) corresponds to the ray. The part of region R close to the outer circle refers to scatterers very close to the source and the geophone, seen under a small offset angle.

The parameter a can be related to the normalized offset wavenumber H (Deregowski and Rocca, 1981; Claerbout, 1985):

$$H = \frac{k_h\, c}{2\omega}. \tag{17}$$

Following that notation and now using migration terminology, that is $h =$ half offset, $t =$ time of arrival of the reflection, we have:

$$H = \frac{2h}{ct}\sin^2\theta = \frac{k_h\, c}{2\omega}. \tag{18}$$

However, in our present notation, $a = ct/2h$. Thus, equating u with k_x, and v with k_z, we have :

$$p = \sqrt{k_z^2+k_x^2}\,\frac{c}{2\omega} = \sqrt{1-\frac{H^2}{\sin^2\theta}} = \frac{1}{\sqrt{1+\frac{k_h^2}{k_z^2}}}, \tag{19}$$

an expression that we also find in Clayton (1981). Up to now, this formula was explored for high values of the parameter a, i.e. close to zero offset (Stolt, 1978). We are, however, interested in the opposite situation, one in which the parameter a is close to, but higher then 1: the analysis of the unperturbed arrival. Referring to Figure 5, we have dashed the region relative to the usual reflection experiment. We will call the dashed region the B (Born) region. It is delimited by the circumference $p = 1$, and by the value of a that corresponds to a reasonable maximum half offset angle, say 45^o. The dotted region that we shall call region R (for Rytov), extends from the origin of the coordinates to a smaller value of a, that we will now take to be equal to 1.1. This region corresponds to waves that arrive in a short time window (10% of the traveltime) after the time of arrival of the unperturbed wavefield. We have already seen that the area in the two circles hatched in Figure 5 (a smaller then 1) corresponds to non-causal arrivals. This can be seen again, when the gradient of the function in equation (11) is considered with respect to ω. This will give us the delay of the wave with respect to the unperturbed arrival, if the traveltimes are so scaled that the direct arrival arrives at time 1. We then have:

$$-\frac{\partial\phi}{\partial\omega} = \frac{\sin\theta}{\sqrt{1-p^2}} = a. \tag{20}$$

The imposition of $a > 1$, is required since we are discussing the effects of scatterers in an uniform medium. Therefore, the conclusions of this section on the geometry of the monochromatic backprojections are the following:

1.) For physical experiments, the amplitude of the backprojection is zero in the hatched area of Figure 5.

2.) The spectrum of the monochromatic ray that links source and geophone is non-zero along the straight line u=0, but not only there. It corresponds to the horizontal raypath y=0.

In fact, the spectrum extends far outside the line $u=0$. If we look at the region labeled as R, it appears that the spectrum of the wavefield, time windowed after the unperturbed arrival, extends to the region close to $p=1$, even for values of a close to 1. This is theoretically correct, but we have to notice that this part of the region R refers to scatterers close to source and geophone, and seen under a very small offset angle. Thus, we can neglect this part of the spectrum since it does not refer to the medium spanned by the ray.

If we do not time window the arriving wave immediately after the unperturbed arrival, but encompass progressively all the successive time events, then the 2-D spectrum of the ray will get wider and wider before arriving at the unit circle ($a=\infty$) . In conclusion, the actual spectral width of the ray is not well-defined on the basis of the considerations that we have made up to now. This point will be discussed in the next section.

WIDEBAND BACKPROJECTIONS; RAYS

Multifrequency experiments

Let us suppose that we have a pure delay multi-frequency, wideband experiment, as usual in seismics. In other words, at the geophone location, we are able to measure the phase of the scattered field at several frequencies. Let this phase be:

$$\phi_s = -\frac{\omega L}{c} \; ; \; L = aD. \tag{21}$$

Then we measure an impulsive wave shape. To get a picture of the scatterer's distribution that is consistent with the phase measurements, we have to combine several monochromatic backprojections.

An easy way to be able to evaluate the answer is to total the corresponding backprojections for different values of ω , and to use the stationary phase principle for that. For each frequency, the phase of the estimated scatterer is:

$$\phi_0(\omega) = -\frac{\omega L}{c} + \frac{\omega D}{c}\sin\theta\sqrt{1-\frac{c^2\rho^2}{4\omega^2}}. \tag{22}$$

Substituting for ω from the stationary phase equation

$$\frac{\partial\phi}{\partial\omega} = 0 \; ; \; \omega = \frac{\rho c}{2}\times\frac{1}{\sqrt{1-\frac{\sin^2\theta}{a^2}}}, \tag{23}$$

$$\phi_0 = -\rho\frac{D}{2}\sqrt{a^2-\sin^2\theta}. \tag{24}$$

This phase function will anti-transform into the usual migration ellipse. The amplitude distribution across the ellipse depends on the relative weights given to different frequencies, and therefore to the source wavelet.

It is also evident that, if we did not have an impulsive arrival, but rather had dispersion, we would have back-projected that measurement into a dispersed ellipse, one which depended upon the phase vs. frequency behavior of the measured direct arrival. It is relevant to observe that for $a=1$, that is for the unperturbed ray, the stationary phase approximation of the anti-transform gives two spikes located at the source and geophone and not, as we might have wished, the line linking S and G.

In conclusion, to be able to calculate the width of the ray, we need further analysis. The analysis is carried out in the next section.

The width of the ray

Let us suppose that the phase measured at the geophones exactly matches the traveltime correspondent to the unperturbed arrival. This implies that we know that the medium is devoid of scatterers in a region that is comprehensive of source and geophone. How wide is that region and does it depend on the central frequency of the radiation? In this section, we show a simple way to answer this relevant question. We calculate the backprojections at different frequencies, and total them without considering frequency dependent weights. Therefore we neglect effects due to the jacobian or to the source wavelet. The modulus of the sum of the backprojections, in the spatial domain, will be seen to converge rapidly to zero outside a region whose width will be calculated.

We use for the backprojection in the spatial domain the product of the Green's functions, centered in S and G. The Green's functions change a little depending on the dimensionality of the space, but this effect will be seen to be minor. To avoid confusing calculations, we evaluate the backprojections only along the axis of the segment connecting S and G. If we use the asymptotic expansion of the Green's function in space, we see that the phase of the monochromatic backprojection is, in the location distant d from the SG line ($d \ll D/2$) (fig. 6),

$$\phi = -\frac{\omega}{c} \times [D - \sqrt{D^2 + 4d^2}]. \tag{25}$$

Averaging the frequencies in the bandwidth we have that the multifrequency backprojection $B(d)$ is, if $\Omega_{\min}$ and $\Omega_{\max}$ are the frequencies edges of the band and if we approximate the square root:

$$B(d) = \frac{1}{\Omega_{\min} - \Omega_{\max}} \times \int_{\Omega_{\min}}^{\Omega_{\max}} \exp(j \frac{2\omega d^2}{cD}) d\omega \tag{26}$$

$$B(d) = \frac{1}{\chi_{\max} - \chi_{\min}} \int_{\chi_{\min}}^{\chi_{\max}} e^{j\chi} d\chi$$

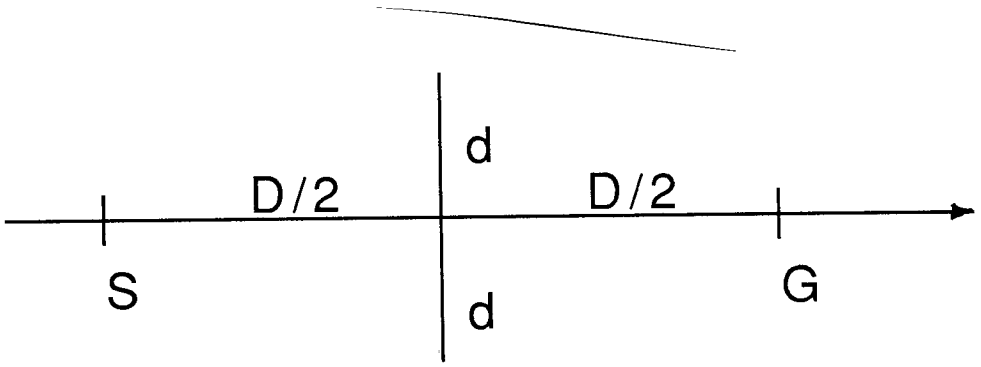

FIG. 6. Spatial width of the wideband backprojection.

$$B(d) = \frac{\sin\frac{\chi_{max}-\chi_{min}}{2}}{\frac{\chi_{max}-\chi_{min}}{2}} \times e^{j\frac{(\chi_{max}+\chi_{min})}{2}} \tag{27}$$

where with χ we indicate

$$\chi = \frac{2\omega d^2}{cD}.$$

We see thus, that the amplitude of the multifrequency backprojection decays much faster then that of the monochromatic one. This happens if all the backprojections have the proper phase. If we take the position of the first zero of the modulus of the sum as the effective width of the wideband backprojection we have:

$$\frac{2d^2}{cD} \times (f_{max} - f_{min}) = 1$$

$$d = \sqrt{\frac{cD}{2B}} = \sqrt{\frac{D\lambda_e}{2}}.$$

Now λ_e is the wavelength corresponding to the bandwidth and not to the central frequency. This also corresponds to the Fresnel zone of the central frequency, in the case where Ω_{min} is equal to 0.

The key point of this section is the following: the width of the multi-frequency backprojection is inversely proportional to the bandwidth. The wider that band, the closer we get to ray theory. The central frequency is irrelevant.

With a quick calculation, we can see that this width is not negligible at all, for seismic data. Let us suppose that the seismic band extends from 10 to 70 Hz; that is, we have an equivalent Fresnel frequency of 30 Hz. If the distance SG is, say 5 km, (in the case of reflected sources, that is the most interesting for our purposes) and if the medium velocity is 2.5 km/sec, then the backprojection width is 600 m. The equivalent beamwidth of the ray is close to 14^o . We should better consider this, prior to backprojecting along very thin lines (0^o aperture) as is usually done in seismic tomography. This fact has been discussed previously (Woodward, 1986; Woodward, 1987).

If we now take into account this width, we know that there is going to be some dispersion, since the variation of the medium velocity will not be negligible on this scale. This entails even wider backprojections; thus we see how informative it should be to measure the actual phase of the windowed wavefield, instead of lumping all these measurements into the single reading of a traveltime.

In conclusion we have indicated that the usual lateral variation of velocity is sufficient to generate enough dispersion of the seismic ray to be measurable. These measurements should be helpful for the inversion. Moreover, the effects of a measurement at a geophone location are backprojected on a very wide area. All this is equivalent to saying that traveltime tomography has to be extended to bandpassed traveltime backprojection, or Rytov approximation.

BORN AND RYTOV APPROXIMATIONS

Up to now, we referred implicitly to the Born approximation. We shall now see that in the case of the analysis of the direct arrivals, or as we shall see later, the direct arrivals of the reflected sources, the Rytov approximation is more valid. Hence, the name given to the region in the spectral domain relative to the direct ray is R region, (for Rytov). This region mostly occupies the space close to the origin of the coordinates, i.e. the low wavenumbers ($\rho = 0$).

Following Slaney (1984), the limits of the two approximations are:

$$L\frac{\Delta v}{v} < \frac{\lambda}{2} \quad (Born) \tag{29}$$

$$\frac{\Delta v}{v} < (\frac{\lambda}{2\pi}\Delta\phi_s)^2 \quad (Rytov). \tag{30}$$

In (29), L is the width of the zone where the velocity v changes. In other words, the velocity variations with respect to the background should integrate to less than a π phase shift for the Born approximation to be valid.

In the case of the Rytov approximation, the integral can be large, but it is the change of phase per unit distance $\Delta\phi_s$ times one wavelength that limits the validity of the approximation. In one case, fast but small changes can be accepted; in the other, big but slow changes are expected.

but slow changes are expected.

In the case of the Born approximation, the background velocity has to follow the real one closely so that the updating velocity field found in the inversion stage, (the gradient), at least has the correct sign. The usual way (Tarantola and Valette, 1982; Kolb et.al., 1986) to solve this problem is to to build up the velocity field starting with the lower frequencies and then progress to the highest, adding more and more wavenumbers. This process can be very slow.

In ray tracing tomography, by contrast, the correction to the velocity field is a linear function of the traveltimes, that are a nonlinear function of the data. With correct time picks, the velocity will be properly corrected and the sign of the update will not be mistaken. We see that it can be useful to merge these two types of corrections so that the convergence to the final solution is as fast as possible. In order to have a correct merger, it is necessary to reconcile traveltime tomography with the wave-equation. This will be carried out using diffraction tomography applied to the reflected sources.

It is easy to see that the Born approximation is very poor in the case of direct arrivals. For example, a layer 100 m thick, that has a velocity 700 m/sec different from the background, will introduce a phase shift to a crossing ray that reaches π at the frequency of 32 Hz (obviously much beyond the Born limit). For these situations, we have to use the Rytov approximation. If equation (30) is satisfied, the Rytov approximation implies that the logarithm of the spectrum of the scattered wavefield, if transformed back in time and convolved with the unperturbed wavefield, is a linear function of the velocities. Using the Born approximation, we backproject the difference between perturbed and unperturbed fields, and the update of the velocity field is linearly related to the input data. Using the Rytov approximation, we backproject in the same fashion the anti-transform of the log of the ratio of the two fields in the frequency domain. To clarify this concept, we give an example of what this means in the next section. In practice, we backproject the unperturbed field scaled with the differential traveltimes, that could be frequency dependent. The update of the velocity field is now non-linearly related to the input data.

Rytov approximation and the traveltimes

Here we summarize the Rytov approximation, and then interconnect it with traveltime tomography. Following Slaney again, the perturbed wavefield is

$$\Psi(r,\omega) = e^{\Phi(r,\omega)}, \tag{31}$$

where Φ is a complex function of space and frequency. If we decompose the wavefield in the frequency domain multiplicatively, we get:

$$\Phi(r,\omega) = \Phi_0(r,\omega) + \Phi_d(r,\omega), \tag{32}$$

where Φ_0 corresponds to the unperturbed field and Φ_d is the differential phase shift, therefore proportional to the differential traveltime. In the case of pure delays, we get:

$$\exp[-j\,\omega\tau(x)] = \exp[-j\,\omega\tau_0(x)]\,\exp[-j\,\omega\tau_d(x)], \tag{33}$$

where the $\tau(x)$'s are the effective traveltimes in the perturbed medium and τ_0 and τ_d are the unperturbed traveltimes and the perturbation, respectively.

The Rytov approximation implies that

$$\Phi_d(r) = \frac{2k_0^2}{\Psi_0(r)} \times \int_{r'} G(r-r')\Psi(r')\frac{\Delta v(r')}{v(r')}dr', \tag{34}$$

where G is the Green's function and $\Psi(r)$ is the incident wavefield and $k_0 = \omega/c$. Let us now suppose that the unperturbed wavefield is a pulse arriving at time $\tau_0(x)$. Decompose the perturbed wavefield measured at the abscissa x in a sum of spikes:

$$r(t, x_k) = \Sigma r_i(x_k)\delta[t-\tau_i(x_k)-\tau_0(x_k)]. \tag{35}$$

In the frequency domain we then have:

$$R(x_k, \omega) = \Sigma r_i\, e^{-j\,\omega\tau_i - j\,\omega\tau_0} \sim e^{j\,\mu(\omega)}. \tag{36}$$

It can be shown (Angeleri, 1983):

$$\mu(\omega) \sim -\,j\,\omega(\overline{\tau} + \Sigma r_m\, r_n\, \tau_m \frac{\sin\omega(\tau_m - \tau_n)}{\omega(\tau_m - \tau_n)}) \tag{37}$$

where

$$\overline{\tau} = \tau_0 + \Sigma\frac{r_i^2\tau_i}{\Sigma r_i^2}. \tag{38}$$

Apart from the term $j\,\omega$ that has to be combined with the Jacobian of the transformation and that can be modified by considerations based on the signal to noise ratio, we see that the wavelet $\mu(t)$ (anti-transform of $\mu(\omega)$) is approximately a pulse with amplitude $\overline{\tau}$, the average differential traveltime, to which several square wavelets are added. The square wavelets have a duration of $2(\tau_m - \tau_n)$ and amplitude $r_m\, r_n\, \tau_m$. Thus, if we use traveltimes only, we neglect these wavelets. Besides, we should evaluate the traveltimes according to (38). Otherwise we can try to determine directly the unwrapped phase characteristic $\Phi_d(r, \omega)$ and log amplitudes from the scattered wavefield and use their antitransforms. Cellular automata techniques for two-dimensional phase unwrapping are now available that could help solve this problem (Ghiglia et.al. 1987).

MULTIPLE SOURCES AND GEOPHONES

If we had several sources and geophones, we could find the results of wave-number domain diffraction tomography again, provided that we had enough of them to be able to generate plane waves or to receive only along plane waves. This is the case for a distribution of geophones and sources all along a seismic line. In the latter situation we have many backprojections, each one of them being a constraint upon the spectrum of the scatterers.

If the constraints are linearly independent, i.e. if the linear transformation is well-conditioned, then we can find the spectrum of the scatterer in this region. This is exactly the plane wave experiment that we considered in the first section. However, we are now in the situation where both α_s and α_g could be perfectly determined; therefore the measurement would refer to a particular point of the object spectrum.

The previous discussions show that it is not really so. A muting velocity v_0 will keep a greater than c/v_0 ; for example, if $v_0=c/\sqrt{2}$ then $a>\sqrt{2}$, so that we recover the spectrum of the object in the region B of Figure 5, only.

Indeed, we could use the direct arrival as we do in refraction statics. Seismologists use normal mode theory to derive information on the vertical layering from the phases of the refracted arrivals. In principle, we could do the same thing in exploration seismics. In light of this it could be interesting to analyze the phases of the refracted waves to see if we could gather more information from their dispersion.

However, the normal industrial practice is to recover the trend of the velocities, that is the low wavenumber region in Figure 5, from velocity analyses that could be generalized to traveltime tomography (Schuster, 1988; Toldi, 1985). This corresponds to using the images of the surface sources (as they are reflected on flat subsurface layers) as buried sources (Mora, 1987; Mora, 1987b). We could investigate the phases of these arrivals, besides their traveltimes.

If we had a perfectly horizontal layer, then the secondary sources would appear all along the thin line in Figure 7. We will not discuss now the problems of ambiguity due to the lateral changes of this layer (Stork and Clayton, 1986, 1987).

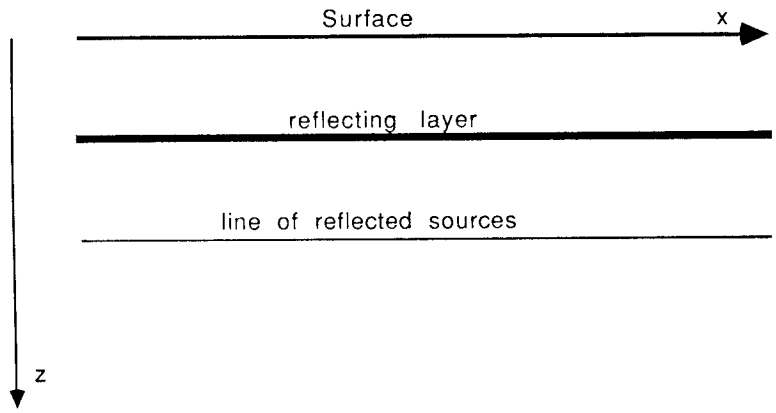

FIG. 7. Surface sources reflected on a flat layer.

Diffraction tomography can be directly applied to this geometry; this is the crosshole geometry (Miller et al. 1987; Wu and Toksoz, 1987), on the folded medium (Fawcett and Clayton, 1984). This geometry could induce us to believe that we could recover the spectrum of the scatterer in a region identical to that hatched in Figure 5. We could then fill the seismic gap in the object wavenumber domain, i.e. the gap between the wavenumbers that can be determined using reflection seismics and those that can be found from extended velocity analyses. Unfortunately, this is not the case, as we shall soon see. Buried sources in a crosshole experiment are much better then reflected sources.

The first problem results from the limitation of the cable length. This limits the observation angles, and therefore delimits the angular width in the spectral domain where we can carry out the inversion. A second problem, also relevant, is that Region B in the spectrum of the secondary source backprojections really corresponds to reflections of reflections: in other words, it describes second order multiples. Even though multiples can be a source of severe problems, they are not sufficiently reliable that we can count on them to carry out an inversion.

Later signals may not be due to reflections coming from the source reflecting on the same layer, but most probably from completely different types of arrivals, i.e. reflections of the same source but on other layers, and therefore equivalent to different sources. In fact, we must not mix travelpaths correspondent to the same (reflected) source and different scatterers with travelpaths corresponding to different (reflected) sources. Hence, to select the proper events, the wavefield has to be windowed in a rather short time window after the arrival of the reflection. Alternatively, one could use wavefield decomposition techniques like those proposed by Harlan (Harlan, 1988).

If we limit this window to say, 10% of the traveltime, we conclude that we can expand the domain of inversion relative to traveltime tomography, but not as much as we would have liked. The situation is much better if we can use reflected sources up to $a = \sqrt{2}$. In Figure 8 we show the spectrum of the backprojections of reflected arrivals windowed with $a = 1.1$ (A) or $a = \sqrt{2}$ (B). The downgoing rays make an angle with the vertical smaller than 30^o. To avoid a cluttered picture we have restricted the beamwidth of the backprojection to 30^o.

We have to remark here that P. Mora (1987) in his thesis also used reflected sources for inversion. He also advocated to boost these reflections of reflections by dividing by the reflection coefficient of the flat layer that reflects the source. The very interesting results that he achieved may also be due to the quite noticeable reflection coefficient he hypothesized in his simulation. This effect is illustrated in his Figure 5.6, where the second order multiple appears at about 1 sec traveltime in the middle of the section.

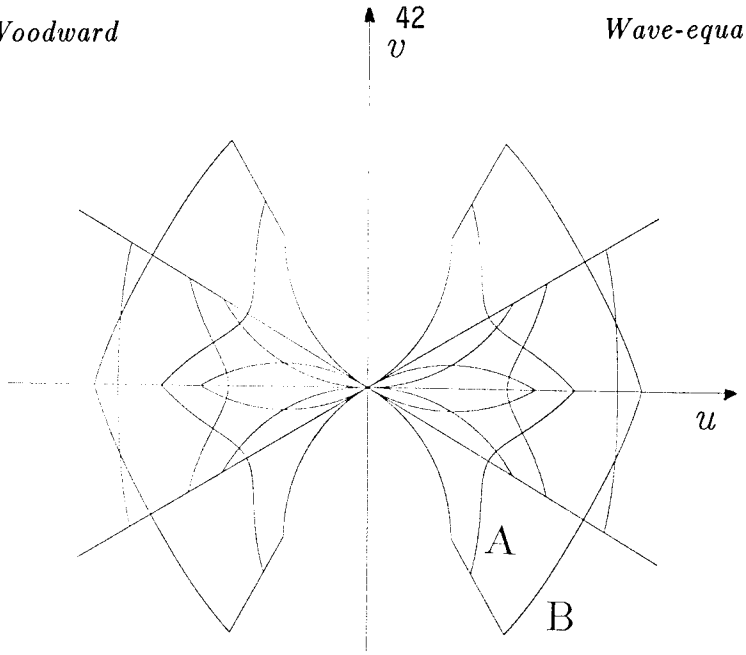

FIG. 8. Spectrum of the backprojection of the reflected arrivals, windowed out after 10% (A) or 41% (B) of the traveltime. Downgoing rays make an angle with the vertical smaller than 30^o .

MODELLING AND INVERSION WITH WAVE-EQUATION TOMOGRAPHY

The analyses carried out in the previous section could have noticeable implications for a better modeling of first arrivals. They might improve upon current ray tracing procedures. First and foremost, it is necessary to average the medium according to equation (27). At the same time, the inhomogeneity of the medium should be taken into account since the backprojections change with frequency. Instead of rapid traveltime variations, we should thus see continuous phase shifts in the modelled data. At the same time, this technique will make clear the impossibility of recovering the spectrum of the object in the null zone; in the case of the analysis of the traveltimes of reflections off plane layers, the width of the null zone has, however, been seen to be dependent on the time windowing of the reflections and therefore upon the presence of other nonrelated reflections. There is no absolute way of finding out how wide this null zone may be. We must examine the real data case by case. Again, the problem of ambiguity between mirror and medium should be studied, too. These observations could simplify the pseudoinversion, and allow introduction of a more physical parameterization of the data.

Several applications can be envisaged: for example passive seismics, refraction data inversion, and the use of wavefields generated by drill bit noise. In these cases, most of the retrievable information comes from the inversion of direct arrivals. These sequences may have great length, so that the phase shifts could be measured with great precision, particularly in the case of harmonic or quasi-harmonic sources.

It will be interesting to see, in these cases, if the Rytov inversion of the phase shifts of the direct arrivals could be more effective than the Born inversion of delayed reflections.

CONCLUSIONS

In this paper, we have tried to analyze the numerous problems that still have to be solved to be able to better use the information carried by direct arrivals and direct arrivals of reflections off flat layers. We were able to calculate the spectrum of the monochromatic as well as the wideband backprojection. We do so not only when the offset is small with respect to the depth of the scatterer, but also in the opposite case, i.e. for the direct ray. Then, we have seen that the Rytov approximation is more convenient and we have seen how this corresponds to analysis of bandpassed traveltimes and log amplitudes. In the seismic range of frequencies, the width of the backprojection of the unperturbed wavefield is nonnegligible; consequently, dispersion phenomena have to be modeled first and inverted thereafter.

In the case of sources reflected by flat layers, we have seen that while they might not be as good as buried ones, they still carry relevant information, besides traveltimes. This information has been neglected up to now. One problem to be addressed very carefully is the ambiguity between reflecting layers acting as laterally-varying mirrors and the lateral variations of the medium.

Hope of filling the seismic gap is very small indeed. However, the feeling that we are not doing all that we could is also very strong. Future research effort should be intensely devoted to analyzing whether it is possible to reap good results from real data, or whether these considerations have to be confined to synthetic examples.

APPENDIX I

Convolution of Green's functions in the frequency domain

Results obtained from the elementary techniques used in the section on the spectrum of the monochromatic backprojection can also be extracted from the observation that the backprojection is the product of Green's functions centered at the source and at the receiver. In the Born approximation, the scattered field is

$$\Psi(r) = \int_{r'} O(r')G(s-r')G(r-r')dr' \tag{AI1}$$

and therefore the backprojection is:

$$B(r) = G(s-r)G(g-r). \tag{AI2}$$

This expression was used in the section that dealt with the width of the ray. We can now calculate, approximately, the Fourier transform of $B(r)$ as the convolution of the spectra of the Green's functions. We shall approximate the result as follows: we know

that the spectrum of the Green's function will peak at the values of k_x, k_y, k_z, satisfying the dispersion equation in three or two dimensions, respectively:

$$k_x{}^2+k_y{}^2+k_z{}^2 = \frac{\omega^2}{c^2} \tag{AI2}$$

$$k_x{}^2+k_y{}^2 = \frac{\omega^2}{c^2}. \tag{AI3}$$

The spectrum in 2-D is:

$$H_2(k_x, k_z) = \frac{1}{\frac{\omega^2}{c^2}-k_x{}^2-k_z{}^2}. \tag{AI4}$$

In three dimensions it is:

$$H_3(k_x, k_y, k_z) = \frac{1}{\frac{\omega^2}{c^2}-k_x{}^2-k_y{}^2-k_z{}^2}. \tag{AI5}$$

Approximating the spectrum with a circular annulus that has width d and radius $1/2$ in our normalization, and calculating the convolution, we see that the intersections of the two annuli are located at (Figure AI1)

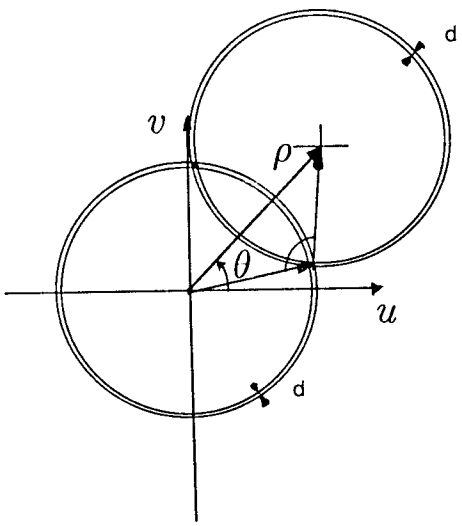

FIG. AI1. Convolution of two Green's functions in the wavenumber domain.

$$u' = \frac{p}{2}\sin\theta \pm \frac{\cos\theta}{2}\sqrt{1-p^2} \tag{AI6}$$

$$v' = \frac{p}{2}\cos\theta - \pm \frac{\sin\theta}{2}\sqrt{1-p^2}$$

The amplitude and phase can be calculated by taking the phase shifts induced by the centering at the source and geophone locations into account, and then evaluating the area A of the intersection (Figure AI2):

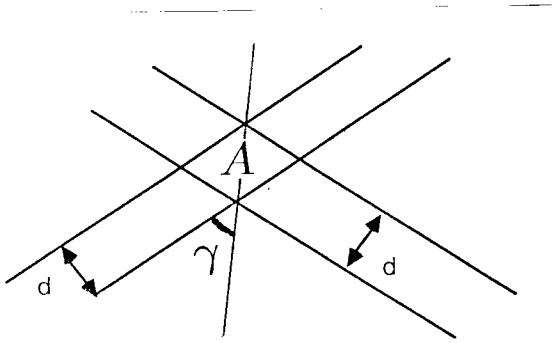

FIG. AI2. Intersection of the two annuli in the wavenumber domain.

$$A = \frac{1}{\sin 2\gamma}, \tag{AI7}$$

where

$$\rho = \frac{2\omega}{c}\sin\gamma \ . \tag{AI8}$$

Thus,

$$A = \frac{1}{\rho\sqrt{1-\frac{\rho^2 c^2}{4\omega^2}}}$$

The results are consistent with those found in the section on monochromatic backprojections. In the case of three dimensions we have spherical shells instead of circular annuli. The volume of the intersection shaped as a torus with the section in Figure AI1 and radius $\sqrt{1-\rho^2 c^2/4\omega^2}$, is proportional to $A = 1/\rho$. This analysis could be made much

more precise along the lines indicated in Wengrovitz et al., (1987), but the coincidence of two approximate results obtained from independent evaluations is useful.

REFERENCES

Angeleri, G. P., 1983, A statistical approach to the extraction of the seismic propagating wavelet: Geophys. Prosp., **31,** No. 5, Oct. 1983, 726 - 747.

Born, M., and Wolf, E., 1959, Principles of optics: Pergamon Press, Oxford

Cheng, G., and Cohen, S., 1984, The relationship betwen Born inversion and migration for common midpoint stacked data: Geophysics, **49**, No 12, Dec. 1984, 2117 - 2131.

Claerbout, J., 1985, Imaging the earth's interior: Blackwell Scientific Publications, London 1985.

Clayton, R. W., 1981, Wavefield inversion methods for refraction and reflection data: Ph.D. thesis, Stanford University, SEP-**27**.

Deregowski, S., and Rocca, F., 1981, Geometrical optics and wave theory of constant offset sections in layered media: Geophys. Prosp., **29**, No. 3, June 1981, 374 - 406.

Devaney, A. J., 1982, A filtered backpropagation algorithm for diffraction tomography: Ultrasonic Imaging, 4, 336 - 350.

Devaney, A. J., 1983, A computer simulation study of diffraction tomography: IEEE Trans. Biomed. Eng., BME 30, 377 - 386.

Fawcett, J. A., and Clayton, R. W., 1984, Tomographic reconstruction of velocity anomalies: Bull. Seis. Soc. Am., **74,** No. 6, , Dec. 1984, 2201 - 2219.

Ghiglia, D. C., Mastin, G. A., and Romero, L. A., 1987, Cellular automata for phase unwrapping: J. Optical Soc. Am. A, **4,** January 1987, 267 - 281.

Harlan, W. S., 1988, A model for phase balancing and velocity filtering: SEP-**57**.

Kolb, J., Collino, F. and Lailly, P., 1986, Prestack inversion of a 1D medium: Proc. IEEE, **74,** No. 3, 498 - 508.

Miller, D., Oristaglio, M., and Beylkin, G., 1987, A new slant on seismic imaging: Migration and integral geometry: Geophysics, **52,** No. 7, Jul. 1987, 943 - 964.

Mora, P., 1987, Elastic wavefield inversion: Ph.D. Thesis, Stanford University, SEP-**52**.

Mora, P., 1987b, Elastic wavefield inversion for low and high wavenumbers of the P and s wave velocities, a possible solution: Deconvolution and Inversion: Bernabini Ed., Blackwell Scientific Publications, London.

Rytov, S.,M., 1937, Diffraction of light by ultrasonic waves: Izv. Akad. Nauk. SSSR, Ser. Fiz. No. 2, 223 - 259. (In Russian).

Schuster, G. T., 1988, An analytic generalized inverse for common - depth - point and vertical seismic profile traveltime equations: Geophysics, **53,** No. 3, March 1988, 314 - 325.

Slaney, M., Kak, A. C., and Larsen, L., 1984, Limitations of imaging with first order diffraction tomography: Inst. Electr. Electronic. Eng. Trans. Microwave Theory and Techniques, **MTT - 32,** 860 - 873.

Stolt, R. H., 1978, Migration by Fourier transform: Geophysics, **43,** 23 - 48.

Stork, C. and Clayton, R. W., 1986, Analysis of the resolution between ambiguous velocity and reflector position for travel time tomography: Presented at the 56 Annual SEG Meeting, Extended Abstract, 545 - 550.

Stork, C. and Clayton, R. W., 1987, Application of tomography to two data sets containing lateral velocity variations: Presented at the 57 Annual SEG Meeting, Extended abstracts, 839 - 842.

Tarantola, A., and Valette, B., 1982, Inverse problems = quest for information: Geophysics, **50,** 159 - 170.

Toldi, J. L., 1985, Velocity analysis without picking: Ph.D. Thesis, Stanford University, SEP-**43**.

Tygel, M., and Hubral, P., 1985, Transient plane wave transforms for the point source seismogram: Geophysics, **50,** No. 12, Dec. 1985, 2889 - 2891.

Wengrovitz, M. S., Oppenheim, A. V., and G. V. Fisk, 1987, Reconstruction of complex-valued propagating wavefields using the Hilbert - Hankel transform: J. Optical Soc. Am., **4,** No. 1, January 1987, 247 -265.

Woodward, M. J., 1986, Iterative tomography: error projection along ellipses and lines: SEP-**48**, 35-43.

Woodward, M. J., 1987, Reflection Tomography: vees in midpoint - offset space, SEP-**51,** 1-12.

Woodward, M. J., 1988, Wave-equation tomography I : SEP-**57.**

Wu, R. S., and Toksoz, M. N., 1987, Diffraction tomography and multisource holography applied to seismic imaging: Geophysics, **52,** No. 1, January 1987, 11 - 25.

LENGTH

48

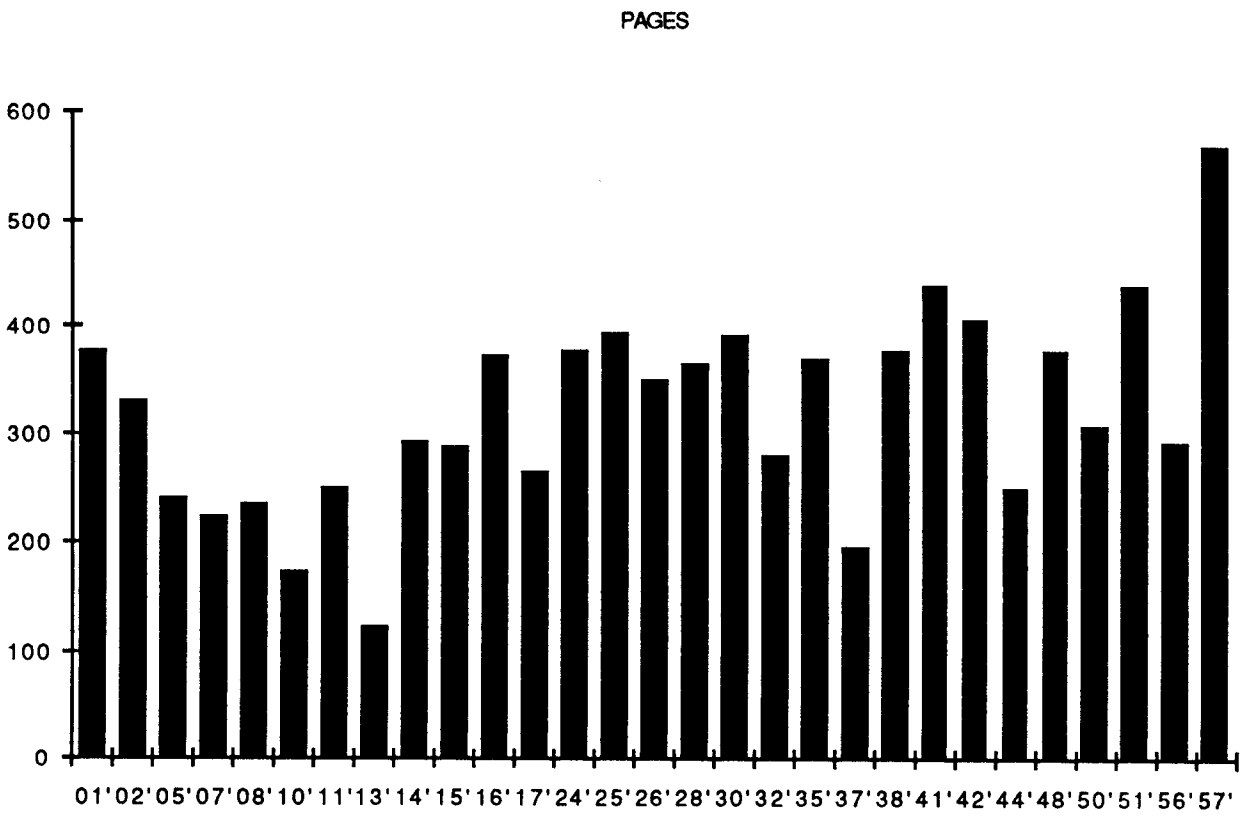
PAGES
600
500
400
300
200
100
0
01'02'05'07'08'10'11'13'14'15'16'17'24'25'26'28'30'32'35'37'38'41'42'44'48'50'51'56'57'